8B.4

WEATHER CALIBRATION EFFORTS ON THE ADVANCED TECHNOLOGY DEMONSTRATOR

Igor R. Ivić* and David Schvartzman

Cooperative Institute for Mesoscale Meteorological Studies, University of Oklahoma, and NOAA/OAR/National Severe Storms Laboratory, Norman, Oklahoma

1. INTRODUCTION

Polarimetric phased array radar (PPAR) technology is being considered as one of the candidate platforms for the next generation of weather radars (Zrnić et al., 2007, Weber 2019). The unique electronic beam steering capability, inherent in PPAR, provides for the enhanced weather surveillance strategies that are envisioned to improve the weather radar products. However, one of the major technical issues related to the use of PPAR technology for weather surveillance is the calibration needed to produce the quality of measurements comparable to the parabolic-reflector antenna systems (Zrnić et al., 2012). Unlike the latter systems, PPARs are plagued with the existence of significant cross-polar antenna patterns which induce cross coupling between returns from the horizontally and vertically oriented fields resulting in the biases of polarimetric variable estimates. Furthermore, the antenna patterns which vary as horizontal and vertical beams are electronically steered in various directions, as consequence produce the scan-dependent measurement biases (Ivić 2018).

Pulse-to-pulse phase coding in either the horizontal or vertical ports of the transmission elements has been proposed to mitigate the cross-coupling effects (Zrnić et al., 2014, Ivić 2017a, Ivić 2017b, Ivić 2018a). This approach, however, does not address the scan-dependent system biases in PPAR estimates. These are caused by the horizontal (H) and vertical (V) copolar antenna patterns which vary with beamsteering direction. The effects of these variations must be addressed via corrections using appropriate values at each boresight location (Ivić and Schvartzman 2019). If the cross-coupling effects are sufficiently suppressed with phase coding and given sufficiently narrow antenna main beam, the corrections can be conducted using only the measurements of the copolar patterns (Ivić 2018b). Furthermore, the effects of active electronic components in transmit and receive paths in PAR systems can result in significant differences between transmit and receive patterns. For these reasons it is important to characterize both transmit as well as receive copolar and cross-polar antenna patterns (Ivić 2019).

Fig. 1. ATD site and the antenna under the radome.

Through a joint collaboration of the National Oceanic and Atmospheric Administration and the Federal Aviation Administration, the Advanced Technology Demonstrator (ATD) was installed in Norman, OK in 2018. This state-of-the-art radar system will be used to evaluate the performance of PPAR for weather observations. It consists of an S-band planar PPAR that is being developed by the National Severe Storms Laboratory (NSSL), MIT Lincoln Laboratory, and General Dynamics Mission Systems (Stailey and Hondl 2016). The main purpose of this system is to serve as testbed for evaluating the suitability of phased array radar (PAR) technology for weather observations (Zrnić et al., 2007).

The ATD antenna was designed by MIT Lincoln Laboratory (Conway et al., 2013) and uses differential-fed single radiating elements (Bhardwaj and Rahmat-Samii, 2014). It is composed of 76 panels arranged as shown in Fig. 1. Each panel consists of an 8×8 set of radiating patch-antenna

* *Corresponding author address:* Igor R. Ivić, 120 David L. Boren Blvd, Room 4415, Norman, OK, 73072; e-mail: igor.ivic@noaa.gov.

elements with dual linear polarization (H and V), for a total of 4864 elements. This arrangement of antenna elements, spaced by λ/2, results in a ~4×4 m aperture which produces a beam that is ~1.6° wide at broadside. On receive, the antenna is partitioned into overlapped subarrays (consisting of 8 panels each) to produce lower sidelobes and suppress grating lobes outside of the main beam of the subarray pattern (Herd et al, 2005). It makes use of pulse compression waveforms to meet sensitivity and range-resolution requirements (Schvartzman and Torres, 2019). The operating frequency band of the antenna is 2.7-3.1 GHz.

The ATD calibration infrastructure includes a far-field calibration tower, located in the vicinity of the ATD site. Atop the tower is an S-band standard gain horn attached to a motorized platform that allows it to rotate about its axis and set the horn polarization in horizontal, vertical or any other desired position. For the purpose of weather calibration, this infrastructure is to be used to conduct accurate antenna pattern measurements of the fielded array. Accurate measurements of copolar patterns can be used to correct the scan-dependent measurement biases.

In this paper, an overview of the latest data correction efforts on the ATD system is presented. Note that the efforts described herein aim at correcting beamsteering biases (i.e., biases relative to a reference point such as broadside) to achieve self-consistency whereby the data bias remains the same for all beamsteering positions (i.e., beamsteering self-consistency). If this is achieved, the ATD calibration reduces to that of a parabolic antenna radar. The paper is structured as follows: In section 2, we present correction methods based on measurements obtained in the anechoic chamber. In addition, we present a statistical evaluation of these corrections using real data collected with the ATD to provide a quantitative comparison between non-corrected and corrected data. Section 3 presents corrections obtained by measuring co-polar and cross-polar patterns using the far-field calibration tower. Section 4 presents an alternative method to derive corrections using weather echoes. The summary is given in section 5.

2. DATA CORRECTIONS USING NEAR-FIELD MEASUREMENTS

Prior to installation in Norman OK, the ATD antenna transmit and receive copolar as well as cross-polar patterns were measured in the near-field (NF) chamber at the MIT-Lincoln Laboratory facilities during March-April 2018 (Conway et al., 2018). The patterns were collected for a total of 2859 electronic beamsteering positions. The beam peaks at all measured locations are shown in *Fig. 2* (left and middle panels). Further, by extracting the copolar beam peaks along the horizontal cardinal plane, the copolar beamsteering biases for Z, Z_{DR} and ϕ_{DP} are computed and shown in Fig. 2 (right panels). Note that the biases are scaled to produce beamsteering biases. These measurements may not represent the current state of the array with utmost accuracy since they were obtained about a year prior to the collection of data analyzed here. Further, the ATD antenna was disassembled and reassembled for transportation and installation in Norman, OK.

Comparing power outputs of each element during the near-field experiment (April 2018) to those with the ATD system fielded in Norman (May 2019) shows little to no increase in failed elements. Specifically, this comparison indicated 11 and 6 additional transmit elements failures on the horizontal and vertical polarizations, respectively. Thus, given the small change in the state of failed elements in the array, and assuming that the radar is sufficiently stable with time and temperature, the near-field measurements are used herein to correct for the copolar biases. Note that we used the NF based corrections to mitigate to the system induced biases relative to the broadside while the absolute calibration values were estimated via the comparison with the collocated NEXRAD radars.

The corrections were tested on data sets collected consecutively on August 13, 2019 via twelve scans, which were mechanically shifted by 10° in azimuth, and at a constant elevation of 0.5°. The overlapping parts of the scans are used to assess the difference in estimated polarimetric variables from collocated volumes illuminated using distinct electronic steering angles (herein referred to as self-consistency). The differences are analyzed when no corrections are applied for the effects of beamsteering and after applying the copolar polarimetric corrections derived from the near-field measurements.

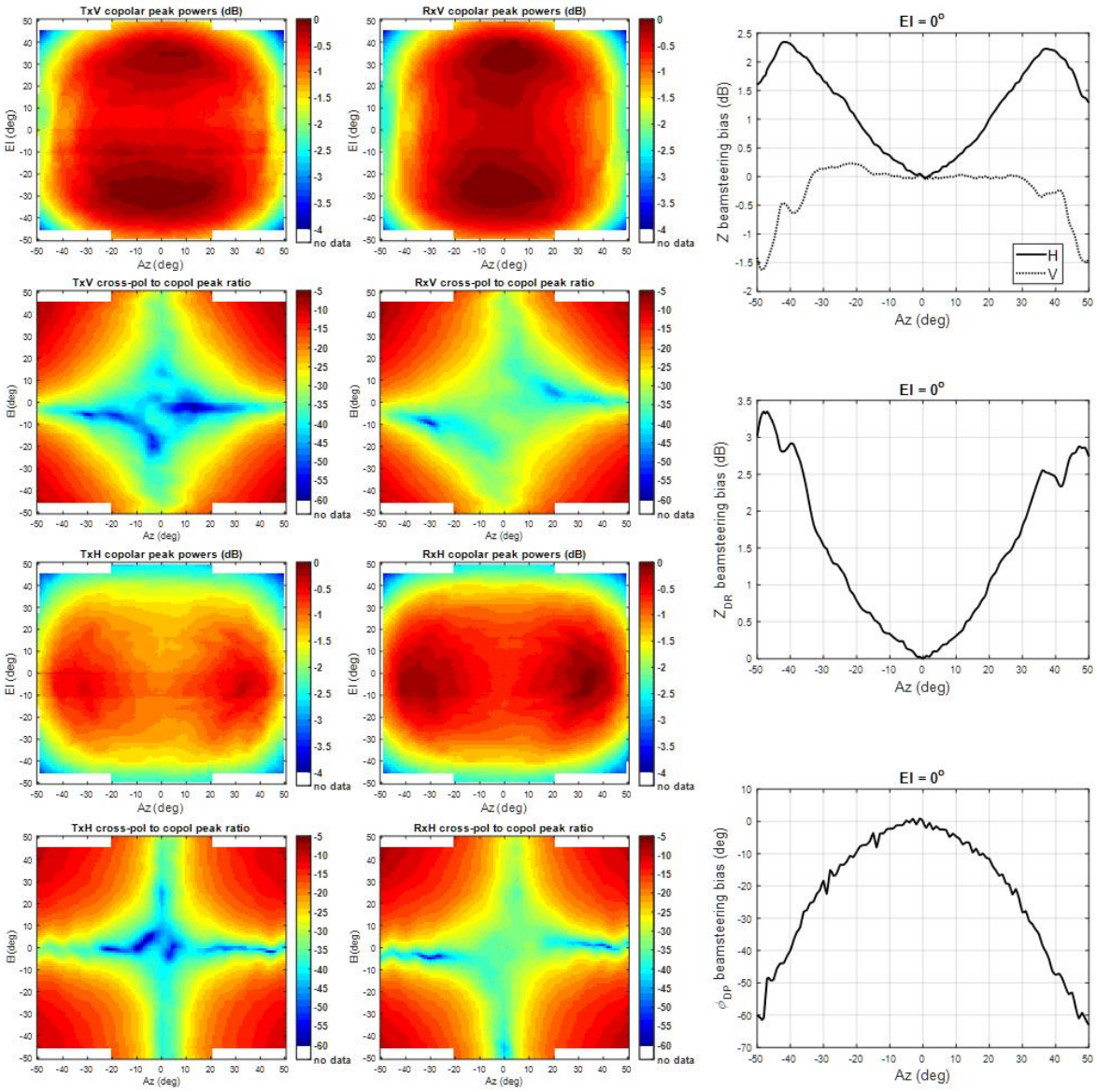

Fig. 2. Transmit (left panels) and receive (middle panels) beam peak powers of the ATD antenna measured in the near-field chamber. Near-field measured copolar beamsteering biases along horizontal principal plane (right panels).

The results before and after corrections are presented in Fig. 3 and Fig. 4. Visual comparison of overlapping areas reveals differences in Z_{DR} and ϕ_{DP} among estimates from different scans in Fig. 3. It is clear that these differences are induced by the system as indicated by the NF measurements (Fig. 2). After applying corrections, the differences are visibly reduced as demonstrated in Fig. 4. Further, the differences at each beamsteering position are averaged in range and shown in Fig. 5 along with differences computed from NF measurements. The weather obtained results for Z are rather noisy and indicate the span of system induced biases of ~±2 dB (dashed line in the upper left panel) while the NF measurements (grey line in the upper left panel) suggest the span of ~±1 dB. Because, the *Z* color scales in Fig. 3 and Fig. 4 are in steps of 5 dB, the system Z biases are not noticeable in the leftmost panels of Fig. 3. In case of Z_{DR} (upper right panel), the overlap between the NF and weather results is clearly visible for azimuths of about ±25° but degrades outside this window. This is also

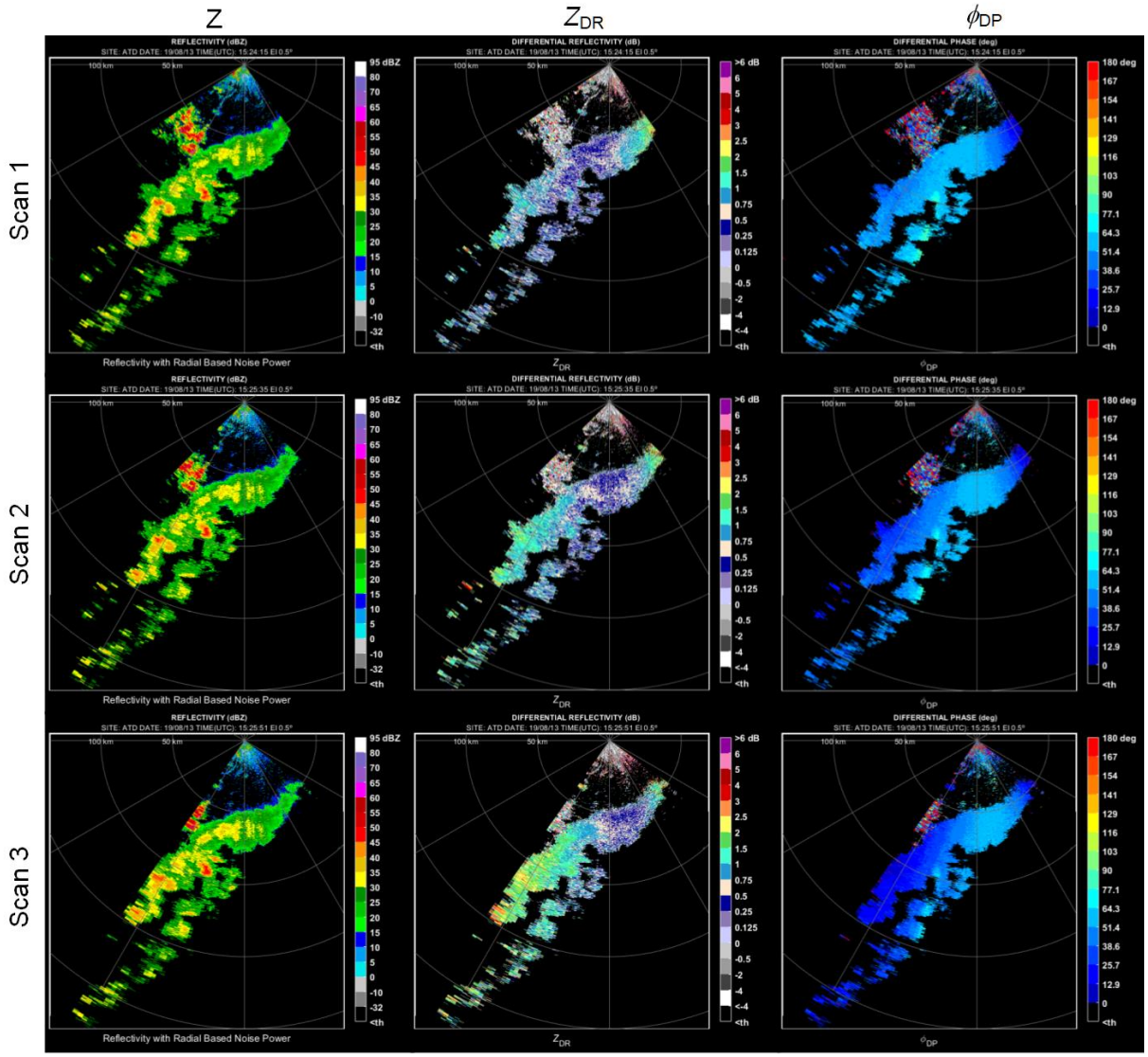

Fig. 3. Raw non-corrected estimates of reflectivity (left) differential reflectivity (center), and differential phase (right) for three consecutive scans shifted mechanically by 10° in azimuth.

corroborated by the weather derived results for the corrected Z_{DR} differences (solid line in the upper right panel) as the fluctuations around zero become larger outside the ±25° interval.

The results for ϕ_{DP} (lower left panel), exhibit the best matching between the weather and NF results. Accordingly, the weather derived differences after corrections exhibit relatively small fluctuations around zero over the entire measured interval. In a broader statistical sense, the benefits of Z_{DR} corrections are demonstrated by the histograms of Z_{DR} differences before and after corrections (the lower right panel in Fig. 5). These show that the histogram before corrections is asymmetric and centered off zero while the histogram after corrections becomes much more symmetric and is centered approximately at 0 dB.

The improvement in the broader statistical sense is further illustrated in Fig. 6 using data that was collected on August 22, 2019. It presents two-dimensional histograms (normalized so that the maximum value is one) of Z_{DR} estimates, before and after corrections, for two scans that are separated in azimuth by 5°, where the time between scans is ~29 seconds. Notice that the histogram of uncorrected Z_{DR} estimates exhibits significant spread (from ~1 to 5 dB) while the histogram produced from corrected estimates

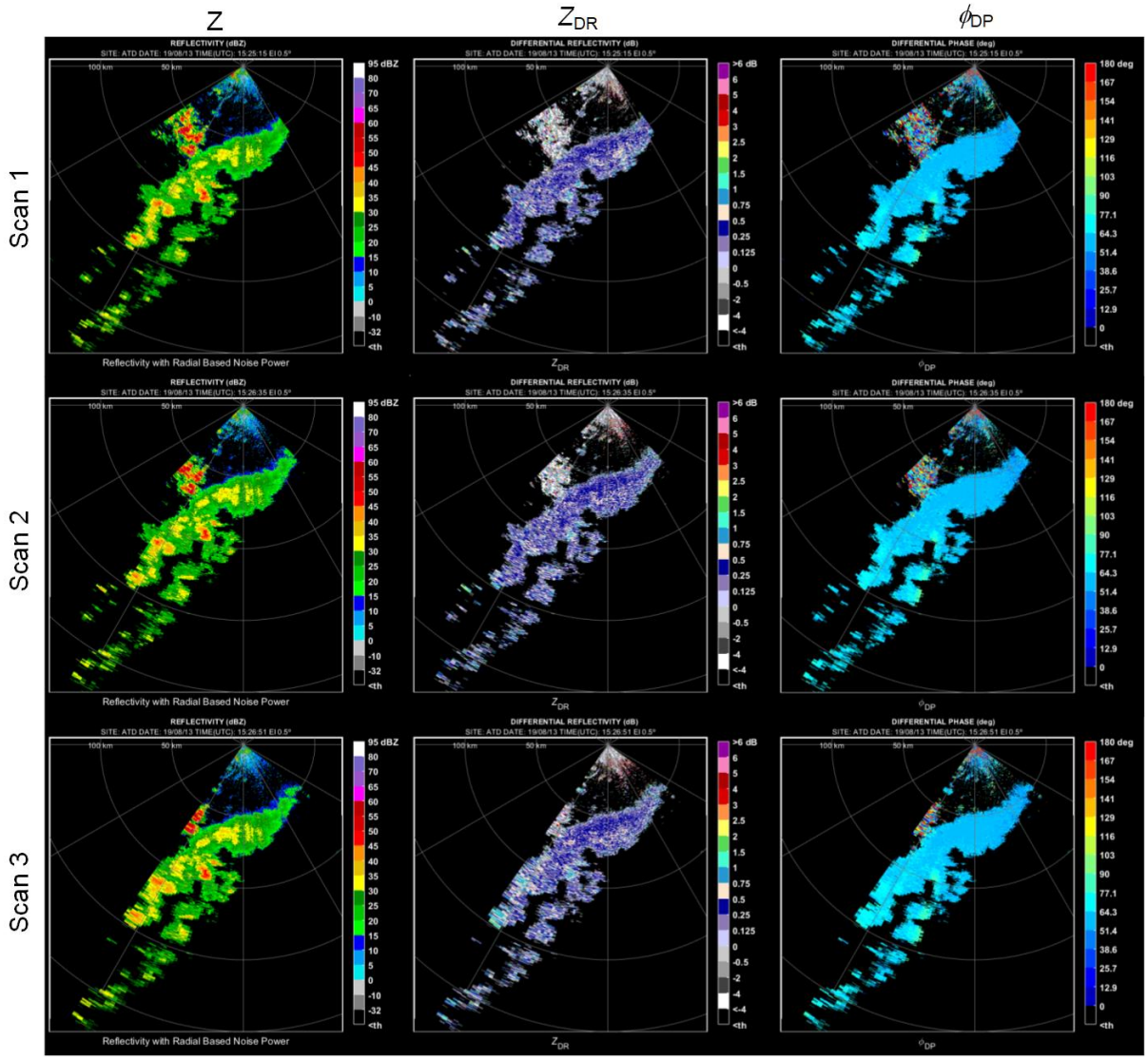

Fig. 4. Estimates after correction using NF measurements (analogous to non-corrected data in Fig. 3).

indicates that the majority of Z_{DR} values in both scans are concentrated at and around 0 dB. This is a clear indication of bias reduction as a result of beamsteering bias corrections. Using ten consecutive weather collections (also collected on August 22, 2019), we further demonstrate the self-consistency improvements by summarizing several histograms of uncorrected and corrected Z_{DR} fields into the boxplot presented in Fig. 7. The mechanical rotation in azimuth and the average time between consecutive scans are 5°, and 28 seconds (exact time difference shown in the *x*-axis labels). With over 100,000 data points used for each box, this shows the robustness and consistency of the corrections from NF measurements. That is, there are significant differences between the 25th, 50th (median), and 75th percentile values of the uncorrected set of box plots (left panel on Fig. 7) before and after the rotation. Additionally, the median Z_{DR} estimates transition from ~1.8 dB to 2.7 dB in a matter of about five minutes. In contrast, the corrected set of box plots (right panel on Fig. 7) shows nearly identical statistical properties for fields estimated before and after the rotation, and the median Z_{DR} estimates more reasonably transition from ~0.9 dB to 1.2 dB in about five minutes.

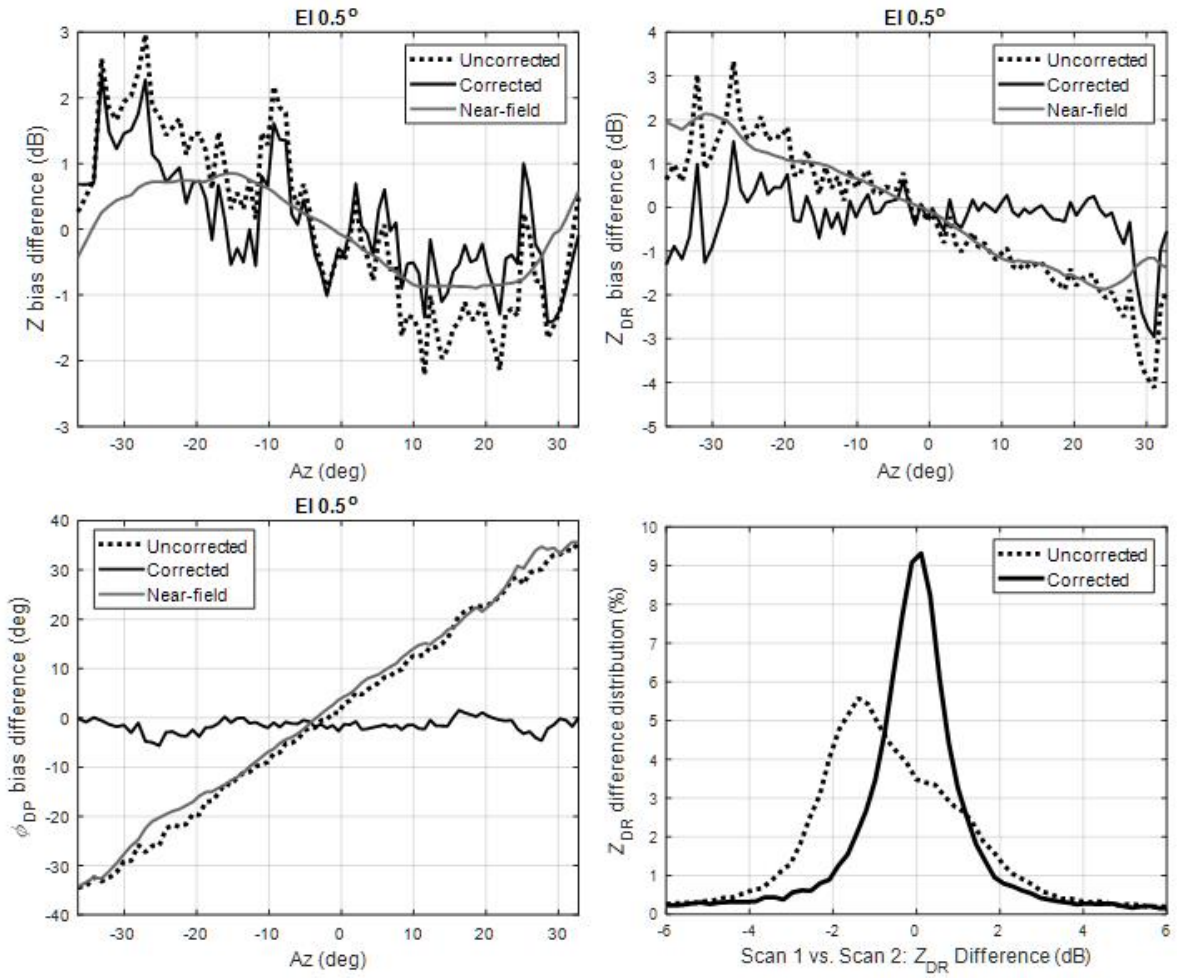

Fig. 5. Range averaged system induced differences among estimates from collocated volumes illuminated during scans 1 and 3 (upper and lower left panels) as well as histograms of Z_{DR} differences before and after corrections (lower right panel).

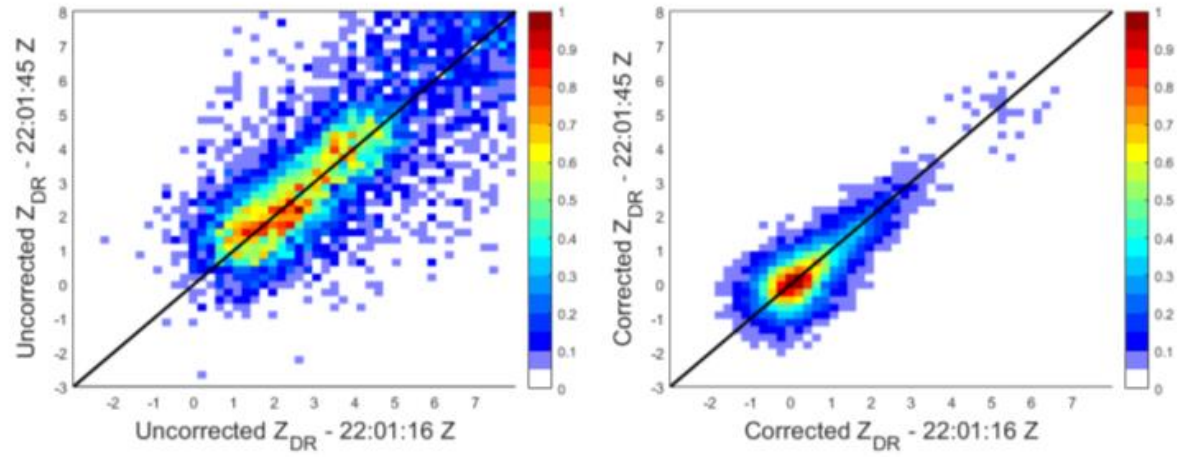

Fig. 6. Two-dimensional normalized histograms illustrate the self-consistency of Z_{DR} estimates between two scans (~29 seconds apart) before and after a mechanical rotation of 5° without corrections (left) and with corrections (right).

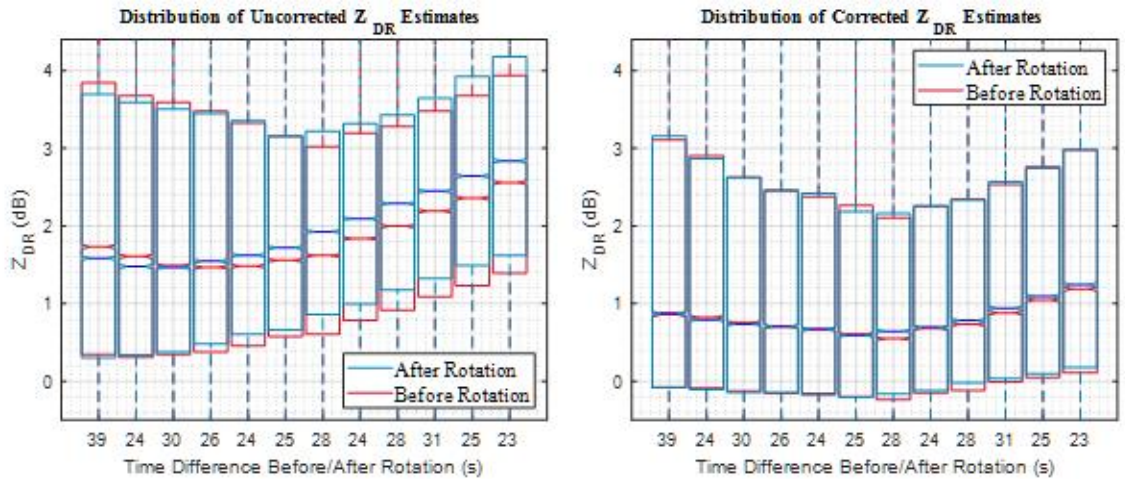

Fig. 7. Boxplots of uncorrected (left) and corrected (right) fields of Z_{DR} from consecutive weather collections. The mechanical rotation in azimuth between consecutive pairs of scans is of 5°, and the average time between consecutive scans is 28 seconds (exact time difference shown in the x-axis labels).

3. WEATHER CALIBRATION USING THE CALIBRATION TOWER

The calibration infrastructure for the ATD includes a 45.7 m far-field calibration tower, located 428 m north of the ATD. Atop the tower, an S-band standard gain horn is mounted at the height of ~45 m. It is attached to a motorized platform that allows it to rotate about its axis and set the horn polarization in horizontal, vertical or any other desired position (Fig. 8). This provides for measurements described in Ivić, 2018b. RF-over-fiber links connect the ATD and calibration tower,

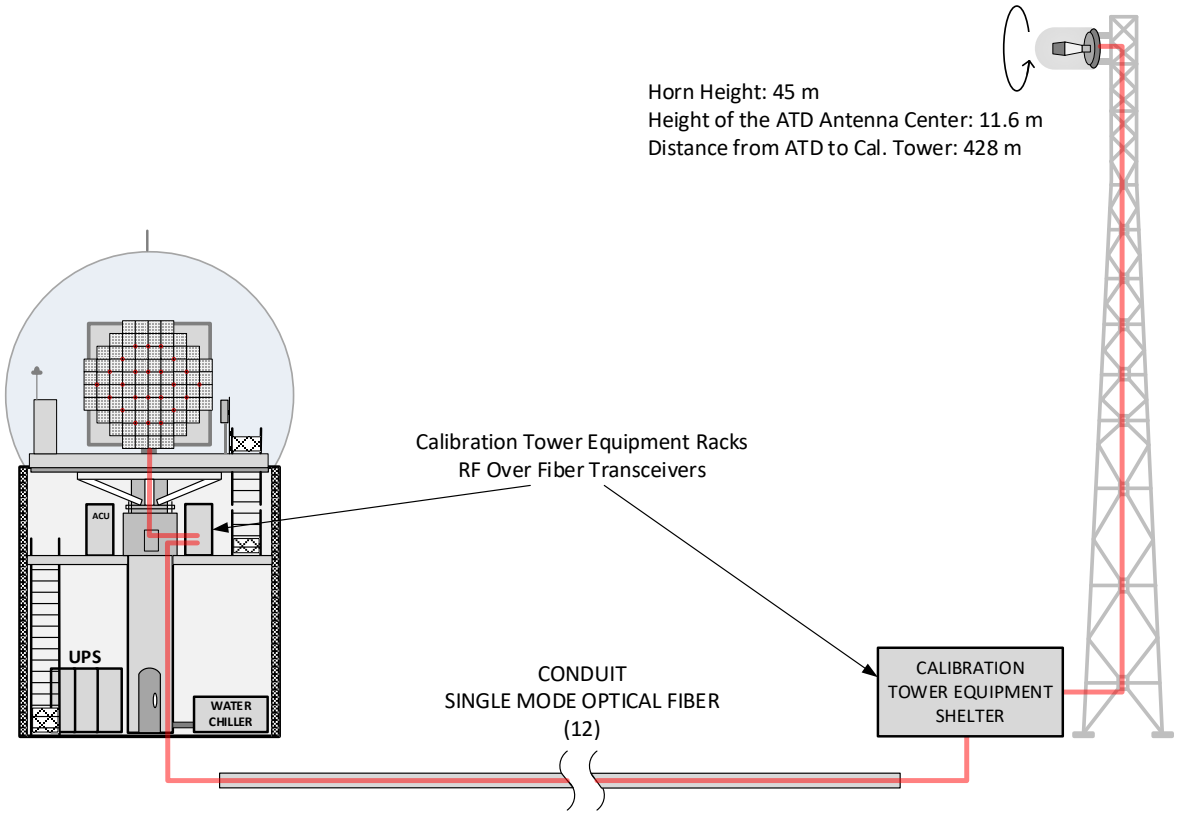

Fig. 8. ATD calibration infrastructure.

allowing coherent calibration. A matrix of switches, attenuators, and amplifiers supports the following multiple modes of measurement: (1) remote horn connected to a continuous-wave source for non-coherent receive measurements

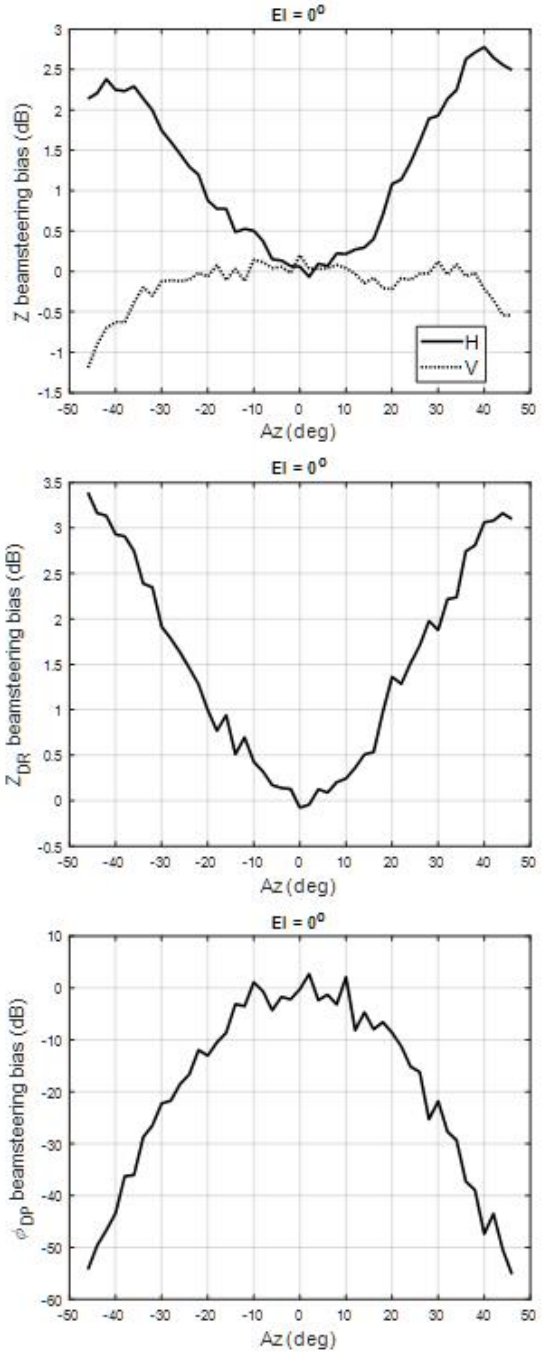

Fig. 9. An example of Calibration tower measurements at elevation 0°. Z beamsteering bias (left panel). Z_{DR} beamsteering bias (middle panel). ϕ_{DP} beamsteering bias (right panel).

of the ATD antenna, (2) remote horn connected to the ATD exciter for coherent receive measurements of the ATD antenna, (3) remote horn connected to the ATD receiver for coherent transmit measurements of the ATD antenna, and (4) remote horn connected to a delay line for two-way measurements. Mechanical positioning of the ATD antenna in azimuth and elevation allows measurements at any steering angle, enabling calibration data to be collected for all electronic scan positions of interest. Hence, the antenna can be mechanically placed in such elevation and azimuth position so that when the beam is electronically steered in the direction to be measured, it points towards the horn location. It is unlikely that the antenna positioning with respect to the horn will be perfect so a box scan will be conducted around the assumed horn location to precisely determine the boresight location which points towards the horn and for which the calibration data is to be collected. This will result in a grid of measurement points with non-uniform spacing. Consequently, an interpolation will be applied to produce correction factors where needed.

This infrastructure is currently being developed and integrated into the ATD system and it will be used to obtain accurate far-field (FF) measurements of the fielded array. Accurate measurements of copolar patterns can be used to correct the antenna induced copolar biases in differential reflectivity (Z_{DR}) and phase (ϕ_{DP}) estimates as well as to correct reflectivity (Z) (Doviak and Zrnić, 1993) as the beam is steered away from broadside (assuming the known system calibration constant for Z at broadside). An example of these measurements is presented in Fig. 9. Further, the described infrastructure will be used to characterize the cross-polar ATD antenna patterns. In combination with copolar measurements, these may be used to create the full correction matrices that account for the copolar biases and mitigate the effects of cross coupling at the same time. These matrices may be used for correction at beamsteering locations where the cross-polar patterns are high and the cross coupling suppression via pulse-to-pulse phase coding is insufficient. cross-polar patterns are high and the cross coupling suppression via pulse-to-pulse phase coding is insufficient.

4. USING WEATHER ECHOES TO ESTIMATE THE BEAMSTEERING BIASES

In addition to the efforts described so far, recent research also explored the possibility of using weather returns to estimate the relative self-consistency corrections curves. To produce such estimates, the radar must be capable to illuminate collocated volumes using distinct electronic steering angles. This in turn, requires the antenna to be mounted on a pedestal as in ATD. Given that this is the most likely operating architecture, this approach (if feasible) may have an operational value. It may be used to validate the existing correction values as well as to aid in the calibration process. An example produced from 10 pairs of ATD scans, where the two scans in each pair are shifted 5° in azimuth with respect to each other, is shown in Fig. 10.

5. CONCLUSION

The weather data correction efforts described here are the first of a kind and have vital importance for the development of PAR technology for weather observations. In that regard, the results of data correction using NF measurements are encouraging because they demonstrate visible improvement in the self-consistency of Z_{DR} and ϕ_{DP} fields. This conclusion is substantiated with statistical results presented in Figs. 5.– 7. These results undeniably demonstrate the benefits of data corrections. This is quite remarkable since the NF measurements were conducted more than a year before data collections and the ATD antenna was disassembled for transportation and reassembled in Norman, OK. Nonetheless, while the NF based corrections exhibit improvements it is unlikely that the applied corrections achieve the beamsteering self-consistency accuracies within the desired limits (e.g., ±0.2 dB for Z_{DR}).

Originally, intended approach to achieve ATD beamsteering self-consistency and calibration is via Calibration Tower. These efforts are ongoing and are troubled with hardware/software issues, equipment instabilities and multipath effects. This is somewhat expected as Calibration Tower efforts are still in the beginning stage.

The third approach is to use weather echoes to estimate the correction data that achieve beamsteering self-consistency. This method can provide a valid correction data estimates only at beam locations where the effects of cross coupling are small or can be sufficiently suppressed (e.g., using pulse-to-pulse phase coding). This method requires further research to establish its usefulness and accuracy.

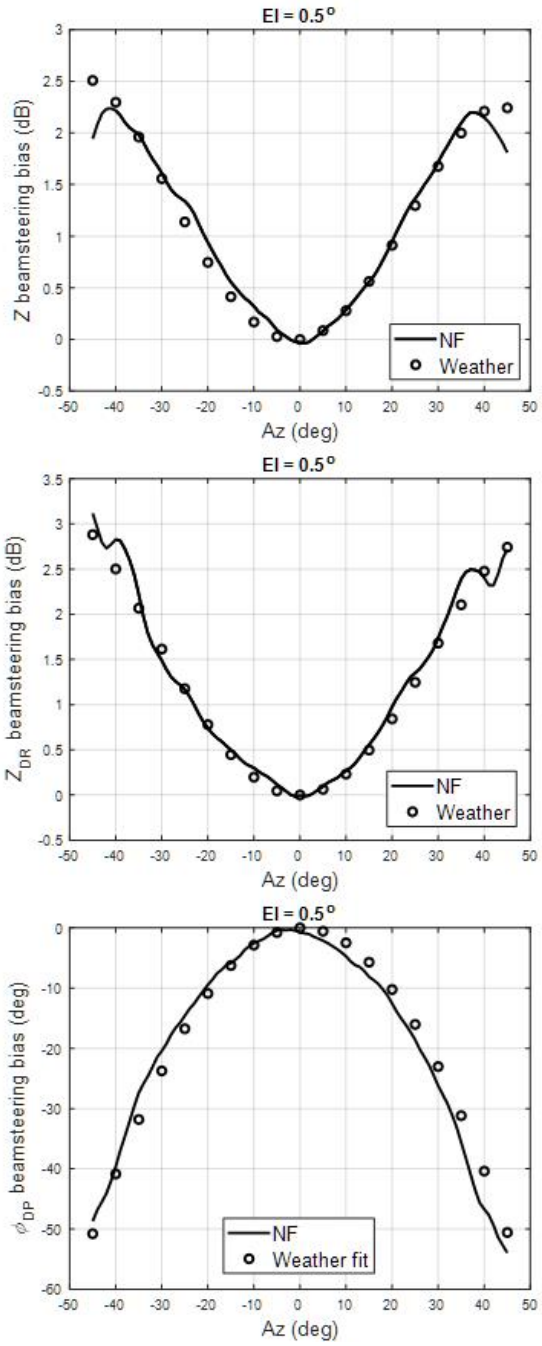

Fig. 10. Results of using weather echoes to estimate the relative system biases for Z (left panel), Z_{DR} (middle panel), and ϕ_{DP} (right panel).

In general, it is encouraging that the correction curves produced using the three methods are all comparable. However, it is yet to be established

whether the corrections that achieve accuracies within desired limits are achievable.

6. ACKNOWLEDGMENT

The authors would like to acknowledge the contributions of numerous engineers, students, scientists, and administrators who have supported these developments over the last decade.

This conference paper was prepared with funding provided by NOAA/Office of Oceanic and Atmospheric Research under NOAA-University of Oklahoma Cooperative Agreement *#NA16OAR4320115*, U.S. Department of Commerce. The statements, findings, conclusions, and recommendations are those of the authors and do not necessarily reflect the views of NOAA or the U.S. Department of Commerce.

7. REFERENCES

Bhardwaj, S., and Y. Rahmat-Samii, 2014: Revisiting the generation of cross-polarization in rectangular patch antennas: A near-field approach. *IEEE Antennas Propag. Mag.*, **56**, 14–38, doi:https://doi.org/10.1109/MAP.2014.6821758.

Conway, D., J. Herd, M. Fosberry, M. Harger, C. Weigand, M. Yeary, and K. Hondl, 2013: On the development of a tileable LRU for the nextgen surveillance and weather radar capability program. *2013 IEEE International Symposium on Phased Array Systems and Technology*, IEEE, 490–493, doi:https://doi.org/10.1109/ARRAY.2013.6731877.

Conway, M. D., D. Du Russel , A. Morris, and C. Parry, 2018: Multifunction phased array radar advanced technology demonstrator nearfield test results. *Proc. of the IEEE,* doi: https://doi.org/10.1109/RADAR.2018.8378771

Doviak, R. J., and D. S. Zrnić, 1993: *Doppler Radar and Weather Observations*. Academic Press, 562 pp.

Herd, J. S., S. M. Duffy, and H. Steyskal, 2005: Design considerations and results for an overlapped subarray radar antenna. Preprints, *IEEE Aerospace Conf.*, Big Sky, MT, doi: http://dx.doi.org/10.1109/AERO.2005.1559399

Ivić, I. R., and R. J. Doviak, 2016: Evaluation of phase coding to mitigate differential reflectivity bias in polarimetric PAR. *IEEE Trans. Geosci. Remote Sens.*, **54**, 431–451, doi:https://doi.org/10.1109/TGRS.2015.2459047

Ivić, I. R., 2017a: Phase Code to Mitigate the Copolar Correlation Coefficient Bias in PPAR Weather Radar. *IEEE Trans. Geosci. Remote Sensing*, *GE-55(**4**)*, 2144-2166, doi: https://doi.org/10.1109/TGRS.2016.2637720

Ivić, I. R., 2017b: An experimental evaluation of phase coding to mitigate the cross-coupling biases in PPAR. *Preprints 38th International Conference on Radar Meteorology,* Chicago, IL.

Ivić, I. R., 2018: Options for Polarimetric Variable Measurements on the MPAR Advanced Technology Demonstrator, *IEEE Radar Conference (RadarConf18)*, doi: https://doi.org/10.1109/RADAR.2018.8378544

Ivić, I. R., 2018a: Effects of Phase Coding on Doppler Spectra in PPAR Weather Radar. *IEEE Trans. Geosci. Remote Sensing*, *GE-56(**4**)*, 2043 – 2065, doi: https://doi.org/10.1109/TGRS.2017.2772962

Ivić, I.R., 2018b: On the Use of Horn Antenna to Calibrate the MPAR Advanced Technology Demonstrator. *10th European Conference on Radar in Meteorology and Hydrology*, Wageningen, Netherlands.

Ivić, I. R., 2019: Facets of Planar Polarimetric Phased Array Radar Use for Weather Observations. *AMS 99th Annual Meeting,* Phoenix, AZ.

Ivić, I. R., and D. Schvartzman 2019: A first look at the ATD data corrections. Preprints, *39th International Conference on Radar Meteorology*, Nara, Japan. Amer. Meteor. Soc., Paper 2-06. https://cscenter.co.jp/icrm2019/program/data/abstracts/Poster2-06_2.pdf

Schvartzman, D., and S. Torres, 2019: Design of Practical Pulse Compression Waveforms for Polarimetric Phased Array Radar. Preprints, *39th International Conference on Radar Meteorology*, Nara, Japan. Amer. Meteor. Soc., Paper 15A-02. https://cscenter.co.jp/icrm2019/program/data/abstracts/Session15A-02_2.pdf

Stailey, J. E., and K. D. Hondl, 2016: Multifunction phased array radar for aircraft and weather surveillance. *Proc. IEEE*, **104**, 649–659, doi: https://doi.org/10.1109/JPROC.2015.2491179.

Weber, M. E., 2019: Meteorological Phased Array Radar Research at NOAA's National Severe Storms Laboratory. *2019 IEEE International Conference on Microwaves, Antennas, Communications and Electronic systems (COMCAS)*. Tel Aviv, Israel.

Zrnić, D. S., and Coauthors, 2007: Agile-beam phased array radar for weather observations. *Bull. Amer. Meteor. Soc.*, **88**, 1753–1766, https://doi.org/10.1175/BAMS-88-11-1753.

Zrnić, D. S., V. M. Melnikov, and R. J. Doviak, 2012: Issues and challenges for polarimetric measurement of weather with an agile beam phased array radar. NOAA/NSSL Rep., 119 pp. [Available online:http://www.nssl.noaa.gov/publications/mpar_reports/]

Zrnić, D.S., R.J. Doviak, V.M. Melnikov, and I.R. Ivić, 2014: Signal Design to Suppress Coupling in the Polarimetric Phased Array Radar. *J. Atmos. Oceanic Technol.,* **31**, 1063–1077, https://doi.org/10.1175/JTECH-D-13-00037.1.